Journal of Materials Chemistry A

Accepted Manuscript

ROYAL SOCIETY OF CHEMISTRY

www.rsc.org/materialsA

Journal Name

RSCPublishing

COMMUNICATION

High Performance H_2 Evolution Realized in 20-μm-thin Silicon Nanostructured Photocathodes

Cite this: DOI: 10.1039/x0xx00000x

Jin-Young Jung,[a] Min-Joon Park,[a] Xiaopeng Li,[a] Jong-Ho Kim,[a] Ralf B. Wehrspohn,[*b] and Jung-Ho Lee[*a]

Received ooth January 2012,
Accepted ooth January 2012

DOI: 10.1039/x0xx00000x

www.rsc.org/

Thickness reduction in high-purity silicon wafers is beneficial for cost-efficient hydrogen evolution utilizing silicon photocathodes. However, two major issues need to be resolved: insufficient light absorption by thin Si absorber and poor charge transfer reaction by dominant surface recombination. Here, we present 20-μm-thin Si photocathodes employing Pt-nanoparticle-coated silicon nanoholes that realize a photocurrent of 23 mA/cm^2 (at 0 V vs. RHE) corresponding to the amount typically achieved by a conventional wafer (~200 μm-thick).

Energy challenges have inspired the use of inexpensive and effective materials for mass production of clean fuels from solar energy. Photoelectrochemical (PEC) cells employing semiconducting materials have attracted considerable interest for directly converting sunlight into storable chemical fuel (hydrogen) via water-splitting.[1-6] Silicon, whose use is prominent in the photovoltaic industry,[11] has appeared as one of the more suitable candidates as a photocathode for H_2 production[7-10] since it has a small band gap (Eg=1.1 eV) that allows for absorption of a large portion of the solar spectrum as well as a proper conduction band height for proton reduction.[12-18] High-purity, moderately-thick (~200 μm) crystalline Si (c-Si) has been utilized for energy conversion with reasonable efficiencies (~10%).[19] The use of thin (<50 μm) c-Si can reduce the material cost associated with Si;[20] however, it has a lower efficiency for PEC water-splitting than thicker (~200μm) materials because thin c-Si films suffer from a notably decreased light absorptance[21] as well as poor PEC performance due to serious surface recombination from thin light absorbers.[22]

To resolve these issues, we have integrated antireflective nanoholes (NHs) on 20-μm-thin c-Si. Then, Pt nanoparticles (NPs) were deposited onto Si NHs (see Fig. 1a). The Pt NPs/Si NHs hybrid structure improved not only light absorptance, but also charge transfer kinetics through effective suppression of surface recombination, which resulted in a high photocurrent for H_2 evolution reaction (HER) on 20-μm-thin c-Si.

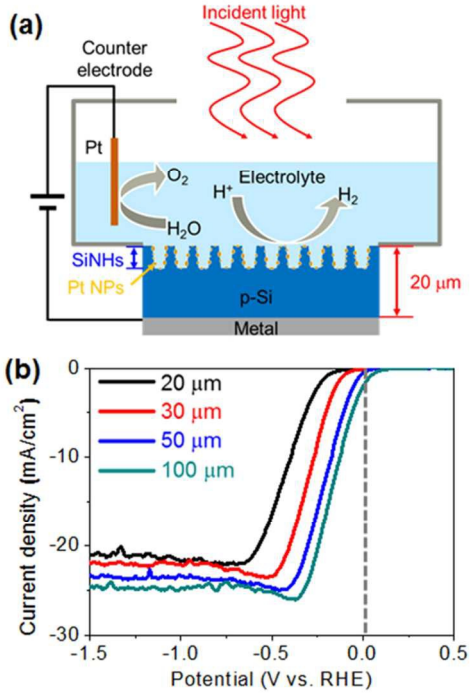

Fig. 1 (a) Schematic diagram of the Pt NPs/Si NHs hybrid as a thin photocathode for H_2 evolution. (b) J-V curves of planar Si as a function of thicknesses (W) at 20 μm (black), 30 μm (red), 50 μm (blue), and 100 μm (cyan).

We characterized the photocurrent density vs. applied potential (*J-V*) responses as a function of thickness (W) of planar Si wafers (Fig. 1b). Compared to 100-μm-thick wafers, the 20-μm-thin wafers showed a reduction in saturated photocurrent density of ~4 mA/cm^2, while the maximum rate for HER was lowered with a cathodic shift of ~320 mV in the *J-V* curve (at 20 mA/cm^2), implying a larger overpotential for

HER. A decrease in W normally causes increased surface recombination with lower light absorptance, resulting in decreased surface minority carrier lifetime (τ_{surf}) representing surface recombination loss according to the following equation:[23, 24]

$$\tau_{surf} = \frac{W}{2S_{eff}} \quad (1)$$

where S_{eff} is a surface recombination velocity.

The onset voltage (V_{os}) is defined as the bias level needed for a photocurrent to exceed the dark current. Our 20-μm-thin wafer exhibited a cathodic shift of ~180 mV compared to the 100-μm-thick wafer (Fig. S1a), which was attributed to a reduction in photovoltage (V_{ph}) owing to a larger surface recombination in thinner c-Si.[25, 26] V_{ph} is related to the effective minority carrier lifetime (τ_{eff}) and photocurrent density (J_{ph}) according to the following diode equation (2):[27]

$$V_{ph} \propto \ln\left(\frac{J_{ph}\tau_{eff}N}{P_i^2}\right) \quad (2)$$

where J_{ph} is the photocurrent, N is the carrier concentration, and P_i is the intrinsic carrier concentration. Thus, lower J_{ph} and τ_{eff} values in thinner c-Si materials leads to a reduction in V_{ph} (see Fig. S1b).

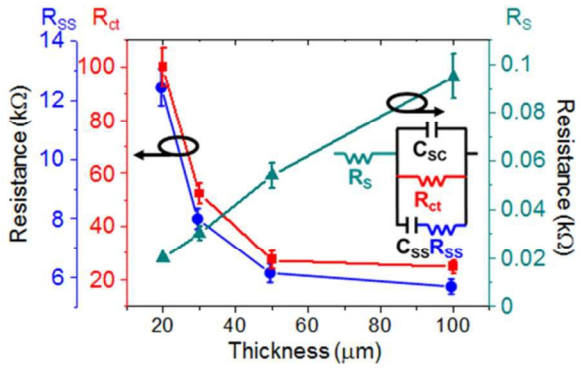

Fig. 2 Representative R_S, R_{ct}, and R_{SS} values determined by best fit with electrochemical impedance spectroscopy results for planar c-Si of various thicknesses (W) from 20 to 100 μm. The inset shows a schematic illustration of equivalent circuits for impedance modeling.

Increased surface recombination in thinner c-Si also causes deterioration in charge transfer kinetics (i.e., larger η for H_2 generation). In our study, charge transfer resistances were analyzed at the semiconductor/liquid interface using electrochemical impedance spectroscopy (Fig. S2). Fig. 2 shows the quantitative values of surface defect resistance (R_{ss}), charge transfer resistance (R_{ct}), and circuit series resistance (R_s), extracted from Nyquist plots by fitting the data into the corresponding circuit. The R_s of photocathodes likely decreased with decreasing W values since the travel distances of charge carriers were normally shorter in thinner substrates. In contrast to R_s, R_{ss} (blue) and R_{ct} (red) values were observed to rapidly increase in wafers thinner than 50-μm due to a higher surface recombination rate.

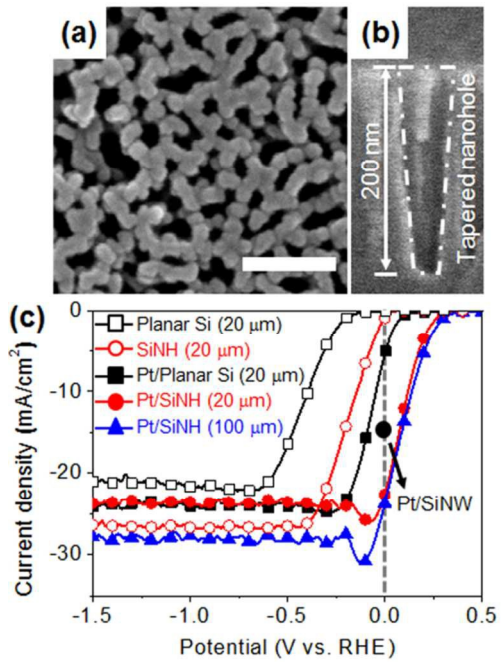

Fig. 3 (a) Top-view and (b) cross-sectional SEM images showing the tapered Si NH array. Scale bar is 100 nm. (c) J-V curves of 20 μm-thick Si photocathodes: Planar Si, Si NHs, Pt NPs/Planar Si, Pt NPs/Si NHs, and 100 μm-thick Si photocathodes for Pt NPs/Si NHs. Filled-circle (black) denotes the highest photocurrent of Pt NPs/Si nanowires at 0 V vs. RHE [Ref. 13].

To improve the PEC performance of thin c-Si photocathodes, tapered Si NHs were integrated using a metal-assisted chemical etching method (Fig. 3a and b)[28] that produced an absorption enhancement in the wavelength range of 300–800 nm (Fig. S3a). For the present study, it should be noted that the highest enhancement of light absorption was obtained with the thinnest c-Si (20 μm) for long wavelengths over 1000 nm, where the light absorption coefficient generally diminishes with decreasing substrate thickness (see Figure S3b). This result might arise from the effective light trapping by tapered Si-NHs where the light scattering could be much more randomized, resulting in an increased light path length.[29] Superior anti-reflectance by Si NHs led to the enhancement of J_{ph} (Fig. 3c) with shifting of the *J-V* curve to a more positive potential (anodic shift of ~360 mV) compared to that of planar Si. This result implied a lower kinetic overpotential for HER in the case of nanostructured silicon. Thus, a larger area of the Si/electrolyte interface may provide a sufficient abundance of activation sites for HER as well as improved interfacial kinetics for charge transfer.[28]

The kinetics of the charge transfer reaction was further improved by the Pt NPs deposited on Si NHs. Previous studies have reported a decrease in NP size as surface morphology reaches a nanostructure scale.[13, 30, 31] For example, under the same deposition conditions NP size decreases to 5~10 nm for rough surfaces in contrast to ~50 nm for planar surfaces.[13] Compared to a planar topology, the overall area of catalytic active sites is considered to be much larger in the case of Pt-coated Si NHs.[13, 30] This finding may indicate that the higher V_{os} of 330 mV in Pt-coated Si NHs (see Figure S4) was due to an improvement in charge transfer kinetics, while the Pt-coated planar sample displayed a V_{os} of 200 mV. As a result, we achieved the highest V_{os} of 330 mV

using a 20-μm-thin wafer, which was almost the same as the value normally obtained from material with a thickness of 100 μm (Fig. 3c). On the other hand, while Pt NP loading significantly improved V_{os}, J_{ph} deceased. It was generally known that a larger conformal coverage of Pt NPs on the surface of Si nanostructures is effective in charge transport, but the photocurrent was greatly reduced due to the light blocking by a large coverage of Pt NPs on the surface of nanostructures.[32, 33] Nevertheless, Pt NPs/Si NHs photocathode could achieve a much higher photocurrent value (23 mA/cm^2 at 0V vs. RHE) than championed value of Pt NPs/Si nanowire photocathode (17 mA/cm^2, see a black, filled-circle in Fig. 3),[13] since Si NHs with a shallow depth of 200 nm could develop a conformal growth of Pt NPs on the surface of Si NHs with minimizing the surface coverage of Pt NPs,[34] compared to Si nanowire with long wire length (>10 μm) which partially covered Pt NPs until about 300 nm depth from end of nanowires tip.[13]

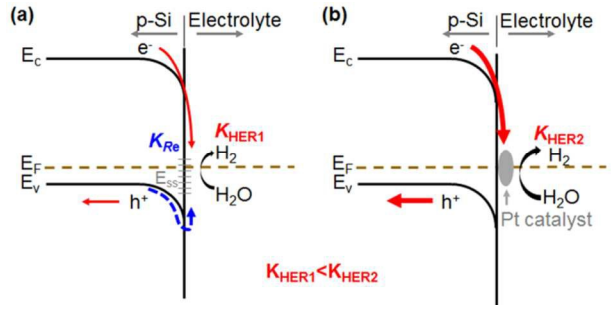

Fig. 4 Schematic illustration showing the band diagram of photocathode for (a) thin c-Si and (b) thin c-Si coated by Pt NPs. Pt NPs facilitate the charge transfer rate for H_2 evolution (K_{HER}) by suppressing surface recombination rate (K_{Re}).

The improvement of PEC performance by Pt deposition stems from the effective mitigation of surface recombination, which is substantial at thinner wafer thicknesses. In PEC systems, the reaction kinetics of charge transfer-to-proton are normally deteriorated due to carrier recombination by surface defects.[23,25] According to equation (1), larger surface recombination is expected for thinner wafers, in turn leading to a rapid surface recombination rate (K_{Re}) and slower charge transfer rate (K_{HER}) as depicted in the energy band diagram (Fig. 4a). Importantly, it should be noted that Pt catalysts can reduce K_{Re} based upon their rapid charge transfer rate (Fig. 4b), since metal has higher energetic states than that of semiconductors, which could also enable facile transport of charge carriers into the metal. Indeed, we observed a remarkable decrease in charge transfer resistance, which was confirmed by employing Pt-NPs at ultrathin wafer thicknesses (Fig. S5). This feature significantly reduced the minority carrier (electron) density at the surface,[26, 35] greatly diminishing the chances for recombination of electrons and holes at the surface trap[2,26] and thus enhancing H_2 evolution.

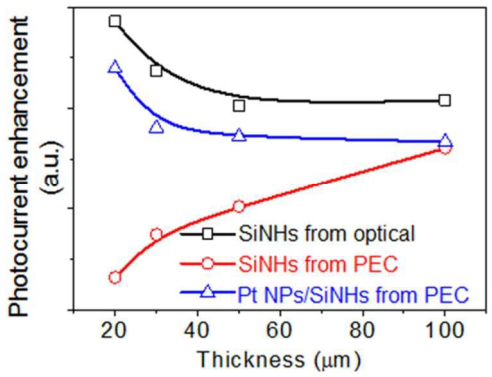

Fig. 5. Photocurrent enhancements of Si NHs and the Pt NPs/Si NHs plotted as a function of wafer thickness.

The superior performance of the Pt NPs/Si NHs hybrid structure was confirmed by the enhancement ratio of the saturated photocurrent. Fig. 5 shows the photocurrent enhancement values, which were calculated by dividing the saturated photocurrent (J_{ph}) values (measured at the saturated region of each sample) by that of the planar silicon value (see also Fig. S6). In principle, the saturated photocurrent is identical to the short circuit current measured at solar cells, which represents the collection efficiency of charge carriers in the photocathode. As wafer thickness decreased, the enhancement ratios of saturated photocurrents in Pt NPs/Si NHs (blue) increased at thicknesses below 50 μm. This trend precisely followed a typical feature plotting the theoretical maximum values of photocurrent enhancement (black), which can be extracted from light absorptance without considering surface recombination loss. In contrast, the photocurrent enhancement values (red) plotted from Si NHs without Pt decreased, which was consistent with our experiments evaluating the effects of decreasing wafer thickness. Thus, it is plausible that the improvement of photocurrent density might be originated primarily from the surface recombination efficiently alleviated by the Pt-NPs/Si NHs hybrid structure. As a result, our Pt NPs/Si NHs hybrid achieved a photocurrent of 23 mA/cm^2 at 0V vs. RHE at the 20-μm-thin wafer, which represents a remarkably enhanced photocurrent performance compared to the championed values of Pt/Si nanowire hybrids (see a filled-circle in Fig. 3).[13,19] In addition, these results suggest the exploration of nonprecious HER electrocatalysts including MoS_2,[36] CoS_2,[37] and $Ni_{12}P_5$[38] as alternatives to Pt catalysts, which may be expected to achieve superior PEC performance while reducing material cost.

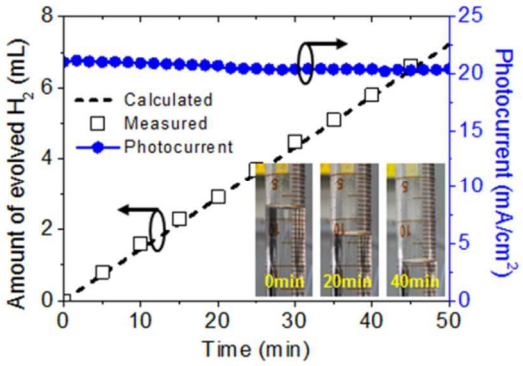

Fig. 6. Hydrogen evolution of 20-μm-thin Si photocathode measured by volume displacement. Black square (measured) and a dotted line (calculated) denote the volumes of collected hydrogen. The inset images show the water meniscus inside a graduated flask pushed down due to H_2 evolution from the top-side of the flask.

Finally, the long-term durability of 20-μm-thin Si photocathodes employing Pt NPs/Si NHs was assessed via chronoamperometry at 0V vs. RHE (Fig. S7). A constant photocurrent of 21 mA/cm^2 was observed over 10 hrs of operation, during which there was sustainable hydrogen evolution on thin c-Si photocathodes. Under a stable generation of photocurrent at 0 V vs RHE, H_2 evolution has been characterized by measuring a volume of H_2 gas collected,[39] as shown Fig. 6. The measured H_2 volumes were well matched with calculated values from the Faraday's law of electrolysis, implying a 100% Faraday efficiency.

Conclusions

In summary, we fabricated 20-μm-thin Si photocathodes employing a Pt NPs/Si nanohole hybrid surface structure for cost-efficient H_2 evolution. Surface recombination became a primary hurdle for lowering photoelectrochemical performance as wafer thickness decreased to 20-μm; however, the Pt NPs coated on the tapered nanoholes successfully resolved this issue. Specifically, the ultrathin (20 μm) wafers exhibited a high photocurrent of 23 mA/cm^2. Thus, our approach suggests a promising route for decreasing the consumption of high-purity silicon for solar-driven water-splitting.

This work was supported by the National Research Foundation of Korea (NRF) grants (No. 2011-0028604) funded by the Ministry of Science, ICT & Future Planning (MSIP). This work was also supported by the New & Renewable Energy of the Korea Institute of Energy Technology Evaluation and Planning(KETEP) grant (No. 20123010010160) funded by the Korea government Ministry of Trade, Industry and Energy.

Experimental section

Si photocathodes were prepared in solar-grade, single crystalline p-type Si (100) wafers with a resistivity of 1–10 Ωcm. A potassium hydroxide solution (30 wt%), which has anisotropic etching behavior towards c-Si, was added at 80 °C to control c-Si thickness via thinning a 200 μm-thickness Si substrate. The Si NH arrays were fabricated in an aqueous solution at room temperature using an MAE method. After dipping thin c-Si into a HF solution to remove native oxide, silver nanoparticles (Ag NPs) were deposited onto Si substrates by dipping into a solution of 99.9% $AgNO_3$ (0.005M) and 49% HF (4.8M). To form vertically aligned Si NH arrays, electroless etching was performed into the solution containing deionized water, HF (4.8M), and 30% H_2O_2 (0.6M) at room temperature. The major morphological parameters such as a filling ratio and a hole depth have been separately controlled by the variation in Ag deposition and etching time. We have found the optimal condition, *i. e.*, Ag deposition time of 1 s and etching time of 15 s, for achieving superior antireflectance while minimizing undesirable surface recombination loss.[28] After electroless etching, Ag NPs remaining on the bottom of Si NHs were removed by treatment with 60% nitric acid for 20 min. Pt NPs were then deposited onto the surface of Si NHs via electroless deposition using a solution containing 0.4 M of HF and 1 mM of K_2PtCl_6 at an optimal deposition time of 9 min (see Figure S8).

To compare the light absorption ability of the Si NH arrays as a function of wafer thickness, the light reflectance (R) and transmittance (T) spectra of Si NH samples were measured using a Perkin Elmer Lambda 750 UV/VIS/NIR spectrophotometer with an integrating sphere. The light absorptance (A) of each specimen was calculated using the relationship A=1–R–T. The photoelectrochemical properties of Si photocathodes were investigated in 0.5 M of 95% sulfuric acid using a solar simulator (Peccel PEC-L11) at AM 1.5G (100 mW/cm^2) illumination after immersion of each specimen into 5 wt% HF to remove native oxides. A three-electrode configuration including the working electrode Si photocathode, a silver/silver chloride reference electrode (Ag/AgCl), and a Pt wire counter electrode were used. The photocurrent spectrum was calibrated by an Si photodiode standard cell (PV Measurements, Inc.). All of the measured potentials vs. Ag/AgCl were converted to the reversible hydrogen electrode (RHE) potentials. To explore several electrochemical properties, electrochemical impedance spectroscopy was performed for photocathodes in the frequency range 0.1 Hz to 2 kHz at 0 V. The obtained EIS spectra were fit to simulated spectra using Z-VIEW software.

Notes and references

[a]*Departments of Materials and Chemical Engineering, Hanyang University, 55 Hanyangdaehak-ro, Sangnok-gu, Ansan, Kyeonggi-do 426-791, Republic of Korea. Fax: +82 31 419 7203; Tel: +82 31 400 5278; E-mail: jungho@hanyang.ac.kr*
[b]*Max-Planck Institute of Microstructure Physics Weinberg 2, D-06120 Halle, Germany Institute of Physics, Martin-Luther-Universität Halle-Wittenberg, D-06099 Halle, Germany. E-mail: ralf.b.wehrspohn@iwmh.fraunhofer.de*

† Electronic Supplementary Information (ESI) available: Onset voltage, minority carrier lifetimes, impedance spectroscopy for planar Si with varying the substrate thickness; Light absorption reflectance spectra for tapered SiNHs; impedance spectroscopy for Pt coated plansr Si. See DOI: 10.1039/b000000x/

1. N. S. Lewis and D. G. Nocera, *Proc. Natl. Acad. Sci. U.S.A.*, 2006, **103**, 15729–15735.
2. M. G. Walter, E. L. Warren, J. R. McKone, S. W. Boettcher, Q. X. Mi, E. A. Santori and N. S. Lewis, *Chem. Rev.*, 2010, **110**, 6446–6473.
3. A. Fujishima, K. Honda, *Nature* 1972, **238**, 37.

4. R. M. Candea, M. Kastner, R. Goodman, N. Hickok, *J. Appl. Phys.*, 1976, **47**, 2724.
5. A. J. Bard, *J. Phys. Chem.*, 1982, **86**, 172.
6. M. F. Weber, M. J. Dignam, *J. Electrochem. Soc.*, 1984, **131**, 1258.
7. D. C. Bookbinder, J. A. Bruce, R. N. Dominey, N. S. Lewis, M. S. Wrighton, *Proc. Natl. Acad. Sci. U.S.A.*, 1980, **77**, 6280.
8. R. N. Dominey, N. S. Lewis, J. A. Bruce, D. C. Bookbinder, M. S. Wrighton, *J. Am. Chem. Soc.*, 1982, **104**, 467.
9. G. Hodes, L. Thompson, J. Dubow, K. Rajeshwar, *J. Am. Chem. Soc.*, 1983, **105**, 324.
10. Y. Nakato, H. Yano, S. Nishiura, T. Ueda, H. Tsubomura, *J. Electroanal. Chem.*, 1987, **228**, 97.
11. D. M. Bagnall and M. Boreland, *Energy Policy*, 2008, 36, 4390–4396.
12. J. H. Oh, T. G. Deutsch, H. C. Yuan and H. M. Branz, *Energy Environ. Sci.*, 2011, **4**, 1690.
13. I. Oh, J. Kye and S. Hwang, *Nano Lett.*, 2012, **12**, 298–302.
14. Y. D. Hou, B. L. Abrams, P. C. K. Vesborg, M. E. Bjorketun, K. Herbst, L. Bech, A. M. Setti, C. D. Damsgaard, T. Pedersen, O. Hansen, J. Rossmeisl, S. Dahl, J. K. Norskov and I. Chorkendorff, *Nat. Mater.* 2011, **10**, 434–438.
15. K. Jun, Y. S. Lee, T. Buonassisi and J. M. Jacobson, *Angew. Chem. Int. Ed.*, 2012, **51**, 423–427.
16. D. V. Esposito, I. Levin, T. P. Moffat and A. A. Talin, *Nat. Mater.*, 2013, **12**, 562–568.
17. M. Lublow, A. Fischer, C. Merschjann, F. Yang, T. Schedel-Niedrig, J.-F. Veyan and Y. J. Chabal, *J. Mater. Chem. A*, 2014, **2**, 12697–12702.
18. X. Wang, K. Q. Peng, X. J. Pan, X. Chen, Y. Yang, L. Li, X. M. Meng, W. J. Zhang and S. T. Lee, *Angew. Chem. Int. Ed.*, 2011, **50**, 9861–9866.
19. S. W. Boettcher, E. L. Warren, M. C. Putnam, E. A. Santori, D. T. Evans, M. D. Kelzenberg, M. G. Walter, J. R. McKone, B. S. Brunschwig, H. A. Atwater and N. S. Lewis, *J. Am. Chem. Soc.*, 2011, **133**, 1216–1219.
20. D. Bae, T. Pedersen, B. Seger, M. Malizia, A. Kuznetsov, O. Hansen, I. Chorkendorff and P. C. K. Vesborg, *Energy Environ. Sci.*, 2015, **8**, 650–660.
21. K. X. Z. Wang, Z. F. Yu, V. Liu, Y. Cui and S. H. Fan, *Nano Lett.*, 2012, **12**, 1616–1619.
22. D. K. Schroder, B. D. Choi, S. G. Kang, W. Ohashi, K. Kitahara, G. Opposits, T. Pavelka and J. Benton, *Ieee T. Electron Dev.*, 2003, **50**, 906–912.
23. J. Oh, H.-C. Yuan and H. M. Branz, *Nat. Nanotechnol.*, 2012, **7**, 743–748.
24. S. Rein, Lifetime spectroscopy: A Method of Defect Characterization in Silicon for Photovoltaic Applications, Springer 2004.
25. X. Yang, C. Du, R. Liu, J. Xie and D. Wang, *J. Catal.*, 2013, **304**, 86–91.
26. R. Liu, Z. Zheng, J. Spurgeona and X. Yang, *Energy Environ. Sci.*, 2014, **7**, 2504–2517.
27. M. Ambrico, R. D. Mundo, P. F. Ambrico, R. d'Agostino, T. Ligonzo and F. Palumbo, *J. Appl. Phys.*, 2012, **111**, 094903.
28. J.-Y. Jung, M. J. Choi, K. Zhou, X. Li, S.-W. Jee, H.-D. Um, M.-J. Park, K.-T. Park, J. H. Bang and J.-H. Lee, *J. Mater. Chem. A*, 2014, **2**, 833–842.
29. K. X. Z. Wang, Z. F. Yu, V. Liu, Y. Cui, S. H. Fan, *Nano Lett.*, 2012, **12**, 1616.
30. K. Q. Peng, X. Wang, X. L. Wu and S. T. Lee, *Nano Lett.*, 2009, **9**, 3704–3709.
31. J. R. McKone, E. L. Warren, M. J. Bierman, S. W. Boettcher, B. S. Brunschwig, N. S. Lewis and H. B. Gray, *Energy Environ. Sci.*, 2011, **4**, 3573–3583.
32. P. Dai, J. Xie, M. T. Mayer, X. Yang, J. Zhan and D. Wang, Angew. Chem. Int. Ed., 2013, **52**, 1–6.
33. K. T. Fountaine, H. J. Lewerenz and H. A. Atwater, Appl. Phys. Lett., 2014, **105**, 173901.
34. M. J. Choi, J.-Y. Jung, M.-J. Park, J.-W. Song, J.-H. Lee and J. H. Bang, *J. Mater. Chem. A*, 2014, **2**, 2928–2933.
35. S. D. Tilley, M. Cornuz, K. Sivula and M. Gratzel, *Angew. Chem., Int. Ed.*, 2010, **49**, 6405–6408.
36. Q. Ding, F. Meng, C. R. English, M. Cabán-Acevedo, M. J. Shearer, D. Liang, A. S. Daniel, R. J. Hamers and S. Jin, *J. Am. Chem. Soc.*, 2014, **136**, 8504–8507.
37. C. Zhao, D. Li, and Y. Feng, *J. Mater. Chem. A*, 2013, **1**, 5741–5746.
38. Z. Huang, Z. Chen, Z. Chen, C. Lv, H. Meng, and C. Zhang, *ACS nano*, 2014, **8**, 8121–8129.
39. S.-M. Shin, J.-Y. Jung, M.-J. Park, J.-W. Song and Jung-Ho Lee, *J. POWER SOURCES*, 2015, **279**, 151-156.

TOC figure

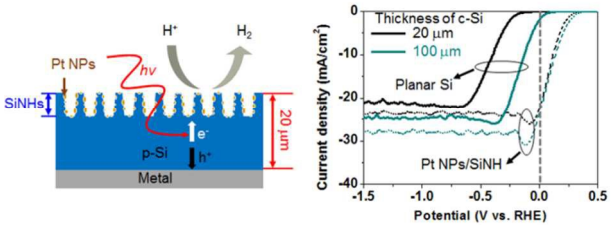

Pt nanoparticles (NPs) are coated on the tapered nanoholes (NHs) integrated using a 20-μm-thin Si wafer. This photocathode significantly improves H_2 production via the efficient light absorption and the suppression of surface recombination for obtaining a high photocurrent value of 23 mA/cm² at 0 V vs. RHE.